

Article

Boron-Based Inverse Sandwich $V_2B_7^-$ Cluster: Double π/σ Aromaticity, Metal–Metal Bonding, and Chemical Analogy to Planar Hypercoordinate Molecular Wheels

Peng-Fei Han ¹, Qiang Sun ² and Hua-Jin Zhai ^{1,*} 

¹ Nanocluster Laboratory, Institute of Molecular Science, Shanxi University, Taiyuan 030006, China; 201722801006@email.sxu.edu.cn

² Center for Applied Physics and Technology, School of Materials Science and Engineering, Peking University, Beijing 100871, China; sunqiang@pku.edu.cn

* Correspondence: hj.zhai@sxu.edu.cn

Abstract: Inverse sandwich clusters composed of a monocyclic boron ring and two capping transition metal atoms are interesting alloy cluster systems, yet their chemical bonding nature has not been sufficiently elucidated to date. We report herein on the theoretical prediction of a new example of boron-based inverse sandwich alloy clusters, $V_2B_7^-$, through computational global-minimum structure searches and quantum chemical calculations. This alloy cluster has a heptatomic boron ring as well as a perpendicular V_2 dimer unit that penetrates through the ring. Chemical bonding analysis suggests that the inverse sandwich cluster is governed by globally delocalized 6π and 6σ frameworks, that is, double $6\pi/6\sigma$ aromaticity following the $(4n + 2)$ Hückel rule. The skeleton B–B σ bonding in the cluster is shown not to be strictly Lewis-type two-center two-electron (2c-2e) σ bonds. Rather, these are quasi-Lewis-type, roof-like 4c-2e V–B₂–V σ bonds, which amount to seven in total and cover the whole surface of inverse sandwich in a truly three-dimensional manner. Theoretical evidence is revealed for a 2c-2e Lewis σ single bond within the V_2 dimer. Direct metal–metal bonding is scarce in inverse sandwich alloy clusters. The present inverse sandwich alloy cluster also offers a new type of electronic transmutation in physical chemistry, which helps establish an intriguing chemical analogy between inverse sandwich clusters and planar hypercoordinate molecular wheels.

Keywords: boron-based inverse sandwich clusters; double π/σ aromaticity; metal–metal bonding; electronic transmutation; chemical bonding



Citation: Han, P.-F.; Sun, Q.; Zhai, H.-J. Boron-Based Inverse Sandwich $V_2B_7^-$ Cluster: Double π/σ Aromaticity, Metal–Metal Bonding, and Chemical Analogy to Planar Hypercoordinate Molecular Wheels. *Molecules* **2023**, *28*, 4721. <https://doi.org/10.3390/molecules28124721>

Academic Editor: Ioannis V. Yentekakis

Received: 8 May 2023

Revised: 9 June 2023

Accepted: 9 June 2023

Published: 12 June 2023



Copyright: © 2023 by the authors. Licensee MDPI, Basel, Switzerland. This article is an open access article distributed under the terms and conditions of the Creative Commons Attribution (CC BY) license (<https://creativecommons.org/licenses/by/4.0/>).

1. Introduction

As a nearest neighbor of carbon in the periodic table, boron features structural diversity and nonclassical chemical bonding, as do its chemical compounds [1]. Elemental boron clusters have been studied both experimentally and theoretically since the 1980s. Anderson and coworkers reported the mass spectra of cationic boron clusters and conducted collision-induced dissociation (CID) experiments, which led to the discovery of magic boron clusters such as B_{13}^+ [2]. Subsequently, the structural and electronic properties of boron clusters have been probed since the 2000s in an array of combined experimental and computational works by Zhai, Wang, and coworkers, in which gas-phase photoelectron spectroscopy (PES) is utilized as a primary technique. These studies showed that anionic boron clusters with up to 40 atoms (excluding B_{39}^-) assume planar or quasi-planar structures [3–14], which represent a highly unusual system in cluster science, being governed entirely by the intrinsic electron deficiency of boron. For cationic boron clusters, planar or quasi-planar structures were observed up to 15 atoms in size, according to ion mobility experiments [15]. In contrast, indirect evidence was revealed for a planar-to-tubular structure transition in neutral boron clusters at around 20 atoms, basing on a joint experimental and computational study on anionic B_{20}^- cluster [16]. The unique geometric structures of elemental boron

clusters are dictated by their chemical bonding, which gives rise to nonclassical concepts of π/σ aromaticity, multiple aromaticity, antiaromaticity, and conflicting aromaticity. The unusual bonding pattern also leads to the dynamic structural fluxionality of bare boron clusters and relevant compound systems.

Doping or alloying with metal elements in boron clusters can effectively tune or alter the structures, electronic properties, and chemical bonding of boron-based alloy clusters. For cases of metal elements with low electronegativity as dopants (such as alkali metals or alkaline earth metals), boron-based alloy clusters should demonstrate intramolecular charge transfers from metal to boron, thus resulting in new types of boron structural motifs that are unknown in bare boron clusters. For transition metals as dopants, the situation appears to be more complicated. Boron-based alloy clusters include a rich variety of geometries: monocyclic boron rings, three-layered sandwiches, half-sandwiches, inverse sandwiches (or anti-sandwiches), tubes, drums, and heteroatomic molecular wheels [17–21]. Indeed, metal-doped boron-based binary clusters have recently emerged as a topic of interest in boron chemistry. In particular, inspired by the planar, circular boron molecular wheels and the high bonding capacity of d orbitals of transition metals, a series of metal-centered boron molecular wheel clusters, $M^{(x)}\text{@}B_n^{k-}$, were designed and experimentally confirmed in recent years: $\text{Co}\text{@}B_8^-$, $\text{Ru}\text{@}B_9^-$, $\text{Ir}\text{@}B_9^-$, $\text{Ta}\text{@}B_{10}^-$, and $\text{Nb}\text{@}B_{10}^-$. These are structurally similar to bare boron wheel clusters, by substituting the central boron site with a transition metal atom [21–24]. On the basis of the electronic requirement for double π/σ aromaticity with $(4N_\pi + 2)$ and $(4N_\sigma + 2)$ electron counting, researchers proposed a design principle that the total number of bonding electrons $(3n + x + k)$ [23] should be equal to $2n + 12$. In other words, the electronic requirement for a central metal atom in anionic $M^{(x)}\text{@}B_n^{k-}$ cluster is $x = 12 - n - k$, where x is the formal valence of a transition metal. Of course, it was assumed here that the metal center exhausts all valence electrons for chemical bonding in the cluster. For a binary system such as the title inverse sandwich cluster, this is not necessarily the case.

Although much progress has been made in the experimental or theoretical studies of transition-metal-doped boron clusters in recent years, there are relatively few works on boron alloy clusters doped with double transition metal atoms. By combining gas-phase PES experiments with quantum chemical calculations, Zhai et al. [25] studied the geometric structure and chemical bonding of a binary Au_2B_7^- cluster in 2006. Subsequently, the studies on Ta_2B_x^- ($x = 2\text{--}5$) clusters by Wang and coworkers and on the Sc_2B_n ($n = 1\text{--}10$) clusters by Jia et al. offered information on the competition between metal–metal, B–B, and metal–boron bonding in alloy boride clusters [26,27]. A joint PES experimental and quantum chemical work on $\text{Ta}_2\text{B}_6^{-/0}$ clusters in 2014 showed that they assume a bipyramidal form, in which a B_6 ring is sandwiched in between two Ta atoms [28], laying the groundwork for more complicated metal-doped $M_x\text{B}_y^-$ -type clusters. This structure may be alternatively described as an inverse sandwich. However, there was no discussion on direct Ta–Ta interaction in the cluster. In a more recent work, Wang and coworkers studied lanthanide-doped boron sandwich clusters, Ln_2B_n ($n = 7, 9$) [29]. A survey of the previous studies of double-transition-metal-doped boron clusters suggests that, except for a Ta_2B_8 cluster [30], it is rather difficult to form obvious metal–metal bonds between metal centers in inverse sandwich clusters.

Can the bimetal unit in boron-based inverse sandwich clusters act as a genuine dimer chemically, instead of two individual capping metal sites? As mentioned above, such examples are rare in the literature. If yes, is there an alternative way to elucidate this kind of novel cluster structure? What governs the structures of inverse sandwich clusters? Why can a monocyclic boron ring exist in inverse sandwich clusters, despite the fact that it is unstable in bare boron clusters? Is there a chemical connection between boron-based inverse sandwich alloy clusters and planar hypercoordinate molecular wheels? What are the peculiar aspects of chemical bonding in inverse sandwich clusters? All these are still open questions to date. In the present contribution, we attempt to address these issues using a properly chosen binary V_2B_7^- cluster as an example. Specifically, we have

computationally designed an inverse sandwich cluster, C_s ($^1A'$) $V_2B_7^-$, through unbiased computer global-minimum (GM) searches and electronic structure calculations at the density-functional theory (DFT) levels. The inverse sandwich cluster is composed of a peripheral monocyclic B_7 ring and a penetrating vertical V_2 dimer. The latter structural unit is shown to possess a Lewis-type two-center two-electron (2c-2e) σ bond, which chemically represents, therefore, a real V_2 dimer. Chemical bonding analysis indicates that the binary cluster is essentially held together by 26 valence electrons that constitute the skeleton σ bonds as well as delocalized 6π and 6σ frameworks. The inverse sandwich cluster shows double $6\pi/6\sigma$ aromaticity, conforming to the $(4n + 2)$ Hückel rule. The overall bonding pattern closely mimics that of a bare B_8^{2-} molecular wheel cluster. We propose that the V_2 dimer in the binary $V_2B_7^-$ cluster, which is formally in the $[V_2]^-$ charge state due to an extra charge in the anion, undergoes electronic transmutation [31,32], so that it becomes a single valence five site (analogous to B^{2-} or C^-). This concept offers a natural chemical connection between inverse sandwich clusters and planar hypercoordinate molecular wheels. There are six extra electrons in binary $V_2B_7^-$ cluster relative to bare B_8^{2-} cluster [6], and they are consumed as a Lewis V–V σ bond and four nonbonding V d electrons (two for each V site, albeit not a lone pair). With this understanding, binary $V_2B_7^-$ and bare B_8^{2-} clusters should indeed be considered isoelectronic, which helps validate the introduction of the electronic transmutation concept into the present alloy cluster system.

2. Results

2.1. Global-Minimum Structure

Alternative optimized low-lying isomeric structures of the $V_2B_7^-$ cluster system are shown in the Supplementary Materials (Figure S1) at the PBE0/def2-qzvp level, along with their relative energies (with corrections for zero-point energies, ZPEs). These low-lying structures are located in this work using the unbiased computer global searches (for both the singlets and triplets). Two additional sets of energetics data are also presented in Figure S1. Firstly, the PBE0-D3/def2-qzvp calculations are conducted for the top 15 structures, which serve to check the dispersion effect on energetics for the current system. Second, comparative B3LYP/def2-qzvp calculations, also for the top structures, are completed to check for computational consistency of different density functionals in terms of geometries and energetics. Note that, in the DFT methods, the PBE0 and B3LYP functionals are widely considered to be complementary to each other for a molecular system. As the results show, all three levels of theory generate highly coherent and consistent energetics data for the system (Figure S1). The GM cluster, C_s ($^1A'$), is reasonably well-defined on the potential energy surface, which is at least ~ 0.6 eV below its nearest C_1 (3A) competitor. This observation suggests that it is rather safe to assign the GM structure. A further benchmark of the energetics (such as at the single-point CCSD(T) level) would not offer much new information for the current system. In this article, we primarily discuss the computational data at the PBE0/def2-qzvp level.

The top and side views of GM C_s ($^1A'$) $V_2B_7^-$ cluster are illustrated in Figure 1. It is a closed-shell electronic system. In the GM cluster, a monocyclic B_7 ring is sandwiched between two capping V atoms, which may be classified as a new example of boron-based inverse sandwich clusters. The C_s GM structure appears to be moderately distorted from a higher D_{7h} symmetry. To address the issue of C_s versus D_{7h} geometries of the system, we have made further computational efforts.

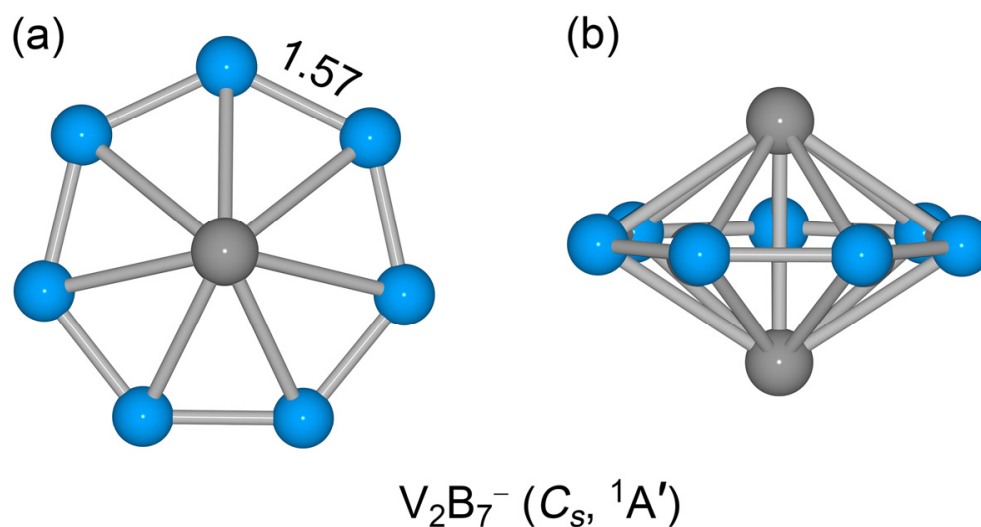


Figure 1. Optimized global-minimum (GM) structure of binary $V_2B_7^-$ cluster at the PBE0/def2-qzvp level. Both (a) top and (b) side views are illustrated. Bond distances of peripheral B–B links (in Å) are also shown.

The $D_{7h} ({}^1A_1')$ structure of $V_2B_7^-$ cluster is confirmed not to be a true minimum at both the PBE0/def2-qzvp and B3LYP/def2-qzvp levels, which are complementary DFT methods as mentioned above. It is a second-order saddle point on the potential energy surface with two imaginary frequencies of $187.2i$ and $182.5i$ cm^{-1} at PBE0/def2-qzvp, as well as $152.3i$ and $146.1i$ cm^{-1} at B3LYP/def2-qzvp. Technically, the $D_{7h} ({}^1A_1')$ structure should be safely ruled out as a minimum for the present system. Nonetheless, the $D_{7h} ({}^1A_1')$ structure only lies 0.008 and 0.009 eV above C_s GM cluster at PBE0/def2-qzvp and B3LYP/def2-qzvp, respectively, which are far within the uncertainties of DFT methods. In other words, the C_s GM and D_{7h} structures are virtually isoenergetic with each other. We believe the distortion of C_s GM $V_2B_7^-$ cluster is very likely a computational artifact of the DFT methods. Chemically, the C_s GM and D_{7h} structures of the system may be viewed as the same geometry. The optimized Cartesian coordinates for the GM $C_s ({}^1A_1')$ and $D_{7h} ({}^1A_1')$ structures of $V_2B_7^-$ cluster at PBE0/def2-qzvp are presented in Table S1.

2.2. Bond Distances, Wiberg Bond Indices, and Natural Atomic Charges

The calculated bond distances, Wiberg bond indices (WBIs), and natural atomic charges of GM $C_s ({}^1A_1')$ $V_2B_7^-$ cluster are shown in Figures 1a and 2, and Table S2; those of $D_{7h} ({}^1A_1')$ cluster are also presented in Table S2. The structural data offer key information for understanding a molecular system. According to the recommended covalent atomic radii [33], the upper bound of bond distance for a B–B, B=B, V–B, or V–V bond is approximately 1.70, 1.56, 2.19, and 2.68 Å, respectively. A typical B=B bond has a distance of 1.52 Å [34]. Based on these reference data, the peripheral B–B links (1.57 Å) in GM $C_s ({}^1A_1')$ $V_2B_7^-$ cluster are apparently shorter than a single bond, suggesting that these are beyond single B–B bond. In line with bond distances, their calculated WBI values (1.29; Figure 2) are clearly greater than 1.00. Thus, the peripheral B–B links are stronger than a single B–B bond, but weaker than a double bond, which is due to the fact that the B–B links have collective contributions from Lewis-type (or quasi-Lewis-type) 2c-2e B–B σ bonds as well as from globally delocalized π and σ frameworks (vide infra).

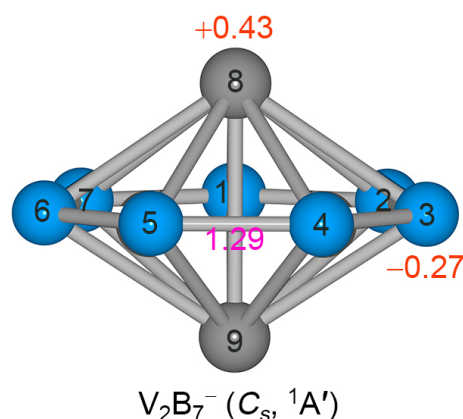


Figure 2. Calculated Wiberg bond indices (WBIs) of peripheral B–B links (in pink color) and natural atomic charges (in $|e|$, red color) for GM C_s (${}^1A'$) $V_2B_7^-$ cluster. These values are obtained from natural bond orbital (NBO 6.0) analysis at the PBE0/def2-qzvp level.

The V–B distances in GM C_s (${}^1A'$) $V_2B_7^-$ cluster range from 2.13 to 2.18 Å (Table S2), which are relatively uniform despite its C_s distortion. The corresponding bond distances in the highly symmetric D_{7h} (${}^1A_1'$) structure are 2.15 Å. In other words, the C_s distortion with respect to D_{7h} is less than 0.03 Å for V–B links, which is relatively minor. The calculated WBIs for V–B links in GM C_s (${}^1A'$) $V_2B_7^-$ cluster are 0.49–0.40 (Table S2), which are substantial considering that each V center is coordinated to as many as seven B atoms and that the V–B bonding is of polar nature. The latter concept is understandable because the B and V elements possess quite different electronegativities: 2.04 versus 1.63. These WBI values demonstrate that the V–B interaction is dominated by covalent bonding. Most strikingly, the V–V distance in GM C_s (${}^1A'$) $V_2B_7^-$ cluster is 2.34 Å, which is somewhat shorter than the upper bound of a single V–V bond (2.68 Å). This observation suggests that direct metal–metal bonding may be present in the inverse sandwich cluster, although a WBI bond order is known to be unreliable for such a bonding situation owing to the occurrence of an intermediate B_7 ring in between two V atoms.

The calculated natural atomic charges from natural bond orbital (NBO) analysis [35] are shown in Figure 2. The B atoms each carry a slightly negative charge of $-0.27 |e|$. The V centers are each positively charged by $+0.43 |e|$. The net charge on a V center seems to be moderate in this anion cluster, again confirming that there is rather covalent V–B bonding. However, it should be noted that the polar nature of V–B bonding is more significant than the above numbers show, because in the anion cluster the extra charge is primarily located on the V_2 unit (vide infra), which effectively compensates for the intramolecular charge transfers from V to B. The actual charge transfer associated with polar V–B bonding is estimated to be around $2 |e|$ in the system. This idea is strengthened using the comparative NBO data from a relevant neutral species, which is described below. In short, the V–B bonding in the alloy cluster, in both anionic and neutral charge states, is of mixed covalent and ionic nature.

3. Discussion

3.1. Chemical Bonding: CMO and AdNDP Analyses, ELF Analysis, and NICS Calculations

In order to understand the unusual geometric structure of GM C_s (${}^1A'$) $V_2B_7^-$ cluster, it is crucial to perform a thorough chemical bonding analysis. To this end, the canonical molecular orbital (CMO) analysis is of fundamental importance. The established bonding picture may be further confirmed or validated using adaptive natural density partitioning (AdNDP) analysis [36]. The GM C_s (${}^1A'$) $V_2B_7^-$ cluster is closed-shell with 32 valence electrons. The 16 occupied CMOs are depicted in Figure 3, which can be classified into five subgroups according to their constituent atomic orbitals (AOs). Subgroup (a) contains seven CMOs. These are primarily composed of B 2s AOs, with secondary contribution

from two V centers. They strictly follow the CMO building principles with 0, 1, 2, and 3 nodal planes from the bottom up, including three quasi-degenerate pairs. The seven CMOs (Figure 3a) can be recombined and localized as a set of Lewis-type or quasi-Lewis-type four-center two-electron (4c-2e) V–B₂–V skeleton σ bonds, one for each peripheral B–B link. Here the localization as seven V–B₂–V σ bonds is necessary because their CMOs involve a nonnegligible component from two V centers (vide infra). The skeleton σ framework consumes 14 valence electrons.

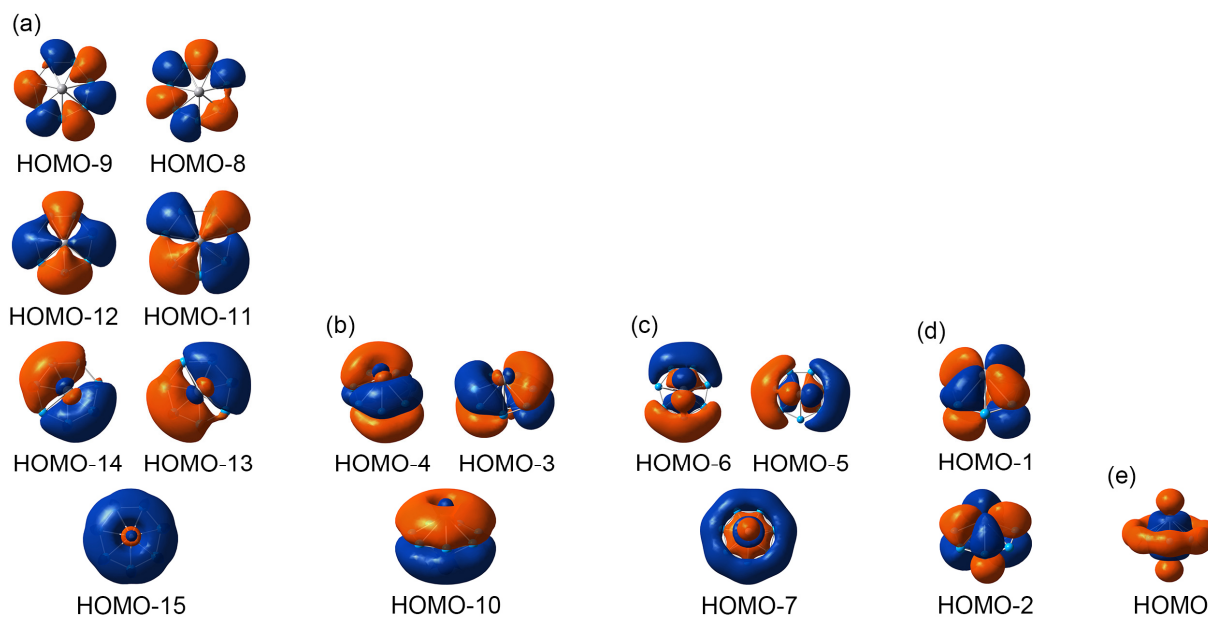


Figure 3. Pictures of canonical molecular orbitals (CMOs) of GM C_s (¹A') V₂B₇[−] cluster. (a) Seven CMOs for peripheral four-center two-electron (4c-2e) V–B₂–V σ bonds; see the text for detailed analysis. (b) Three delocalized π CMOs; that is, the π sextet. (c) Three delocalized σ CMOs. (d) Two nonbonding CMOs over two V atoms. (e) One 2c-2e V–V d _{σ} single bond.

Subset (b) is the global π sextet of the cluster, with a spatial distribution that is closely similar to the prototypical π sextet in benzene. The subset is nine-centered in nature, with contributions from the V₂ unit. The seven-fold symmetry of the inverse sandwich cluster suggests that the π sextet is essentially delocalized and cannot be localized as a Kekulé-type benzene. The 6 π electron counting also conforms to the (4*n* + 2) Hückel rule for aromaticity. Thus, subset (b) renders π aromaticity to the inverse sandwich cluster. Likewise, subset (c) contains three σ CMOs, which are also global in nature. Their overall pattern mimics that of subset (b), except that the former CMOs are σ in nature. Again, these σ CMOs are essentially delocalized and cannot be reduced to Lewis-type σ bonds. It is imperative to claim σ aromaticity for the inverse sandwich cluster, which has 6 σ electron counting that also conforms to the Hückel rule.

The remaining three CMOs in Figure 3, that is, subsets (d) and (e), are mainly based on the V₂ unit and do not involve a major component of either B–B or V–B bonding. This statement lies in the fact that the B₇ ring only represents a quite minor component in these CMOs. The two subsets are discussed in detail in Section 3.2. The above analysis indicates that chemical bonding in the inverse sandwich cluster is dictated by 26 valence electrons, of which 14 are responsible for skeleton σ bonds along the peripheral B₇ ring (with a certain extent of 4c-2e V–B₂–V expansion) and 12 are evenly split between the global 6 π /6 σ frameworks. The inverse sandwich cluster features double 6 π /6 σ aromaticity.

This bonding picture is elegantly borne out from the AdNDP analysis. Our favorable AdNDP scheme is shown in Figure 4. The double 6 π /6 σ aromaticity in the cluster is well-produced in the AdNDP data (Figure 4b,c). The three V₂-based bonding elements are also reproduced in the AdNDP data (Figure 4d,e). For skeleton σ bonding, the 4c-2e

V–B₂–V σ bonds give their occupation numbers (ONs) as 1.98 |e| (Figure 4a), which are nearly ideal values. The 4c-2e V–B₂–V σ bonds are in line with the CMO component data. Our analysis shows that seven CMOs in subset (a) in Figure 3 collectively have a component of roughly ~ 1.7 |e| from the V₂ unit.

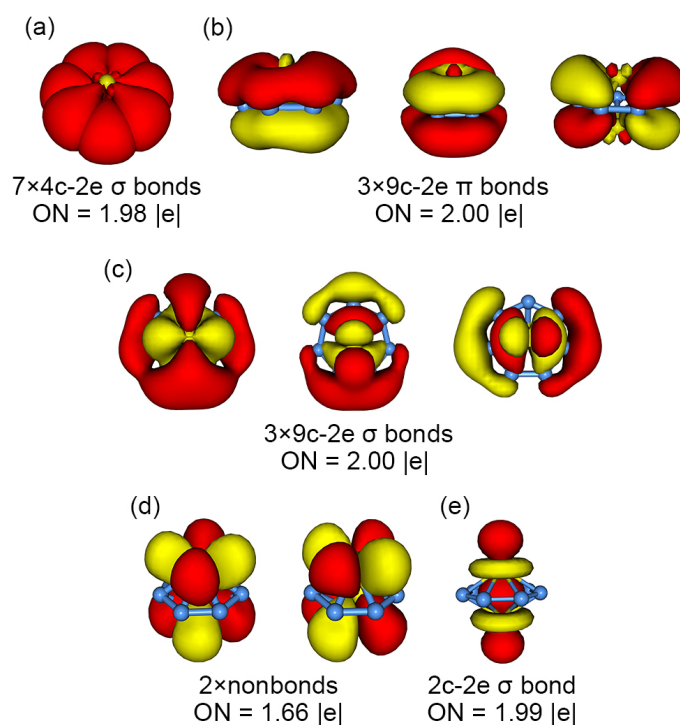


Figure 4. Chemical bonding scheme of GM C_s (¹A') V₂B₇[−] cluster, according to adaptive natural density partitioning (AdNDP) analysis. Occupation numbers (ONs) are indicated. (a) Seven quasi-Lewis-type 4c-2e V–B₂–V σ bonds along the periphery. (b) Global π sextet. (c) Global σ sextet. (d) Four nonbonding V 3d electrons, two for each V center (albeit not a lone pair). (e) One Lewis-type V–V d_{σ} single bond for metal–metal bonding in the system. An alternative AdNDP scheme is presented in Figure S2. The latter scheme is less than ideal, thus highlighting an intriguing difference between inverse sandwich clusters and planar molecular wheels, even in the skeleton σ bonding on the periphery.

Alternatively, the skeleton σ framework can be manually partitioned as seven Lewis-type 2c-2e B–B σ single bonds. Such an AdNDP scheme is shown in Figure S2. The latter AdNDP scheme has fundamental flaws. Firstly, the Lewis-type 2c-2e B–B σ single bonds have relatively low ON values of 1.81 |e| (Figure S2a), which are less than ideal. As a reference, a D_{7h} B₈^{2−} cluster has ONs of 1.95 |e| for its peripheral 2c-2e σ single bonds. Second, as a result of the above artificial partitioning, the corresponding 6π and 6σ bonding elements become highly distorted relative to their CMOs; see Figure S2b,c. The latter observation is an indirect reflection that Lewis-type 2c-2e B–B σ single bonds are not the correct way of partitioning for the system. It is stressed that the roof-like 4c-2e skeleton σ bonds seem to be unique in an inverse sandwich cluster. The electron cloud manages to cover the entire surface of the cluster in a truly three-dimensional fashion, rather than the periphery only. A similar skeleton bonding feature is unknown in planar molecular wheel clusters.

As described above, characteristic double $6\pi/6\sigma$ aromaticity is firmly established in inverse sandwich GM C_s (¹A') V₂B₇[−] cluster from the CMO and AdNDP analyses. To further assess double π/σ aromaticity in the system in a sort of quantitative manner, we calculate the nucleus-independent chemical shifts (NICSs) [37]. It is generally believed that NICS_{zz} is a simple and effective indicator of π/σ aromaticity of a molecular system. As

shown in Figure S3, the $\text{NICS}_{zz}(0)$ values are calculated at the center of the inverse sandwich cluster (that is, the center of the B_7 ring), as well as at the center of the quadrilateral $\text{B}_1\text{B}_2\text{B}_3\text{B}_4$ unit. The $\text{NICS}_{zz}(0)$ values are -70.1 and -74.3 ppm, respectively. In contrast, $\text{NICS}_{zz}(1)$ is calculated at 1 \AA above the center of the quadrilateral $\text{B}_1\text{B}_2\text{B}_3\text{B}_4$ unit, which amounts to -63.4 ppm. Since $\text{NICS}_{zz}(1)$ and $\text{NICS}_{zz}(0)$ roughly probe π and σ aromaticity, respectively, the highly negative $\text{NICS}_{zz}(0)/\text{NICS}_{zz}(1)$ values are a strong indication of π/σ aromaticity in the inverse sandwich cluster.

The calculated electron localization functions (ELFs) [38,39] are also in line with double π/σ aromaticity in the cluster. The ELF_π and ELF_σ data are presented in Figure 5. Note that the bifurcation values for ELF_π (Figure 5c) and ELF_σ (Figure 5b) are 0.94 and 0.76 , respectively, which are all greater than 0.7 , thus indicating double π/σ aromaticity in the system.

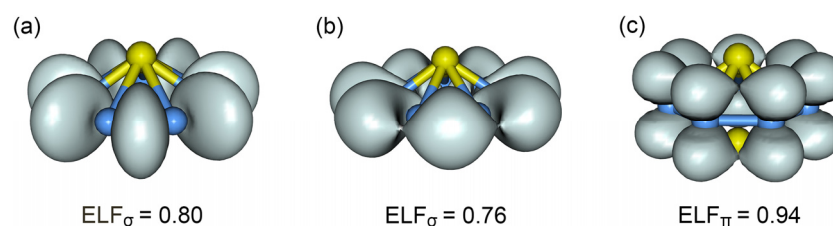


Figure 5. Electron localization functions (ELFs), ELF_σ and ELF_π , for GM $\text{C}_s \text{V}_2\text{B}_7^-$ cluster at the PBE0/def2-qzvp level. (a) ELF_σ associated with seven skeleton σ bonds. (b) ELF_σ associated with delocalized σ bonds. (c) ELF_π associated with delocalized π bonds.

3.2. On the Metal–Metal Bonding in Inverse Sandwich Cluster: Evidence for a $\text{V}–\text{V} d_\sigma$ Bond

The nature of metal–metal bonding in boron-based inverse sandwich clusters has not been sufficiently elucidated in the literature. This issue is of crucial importance in order to achieve an in-depth understanding of chemical bonding in such systems. In Section 3.1, we only briefly mentioned that six of the valence electrons in GM $\text{C}_s ({}^1A')$ V_2B_7^- cluster are primarily based on the V_2 unit. The corresponding CMOs are depicted in Figure 3d,e, whereas their AdNDP bonding elements are shown in Figure 4d and 4e, respectively.

Subset (d) in Figure 3 has two CMOs that are mainly composed of V $3d$ AOs. These AOs are oriented parallel to the plane of B_7 ring. Specifically, HOMO–1 is dominated by V $3d_{xy}$ AOs with a collective contribution of 81% , which is balanced by a secondary B $2p_z$ component. The CMO shows a destructive combination between two V centers, albeit with no direct overlap between their AOs. The coupling between two V $3d_{xy}$ AOs is only formal. The net bonding effect from this CMO is mediated by the middle B_7 ring, with a minor B $2p_z$ component that interacts with both V centers in a constructive (or bonding) manner. Technically, each V center contributes $\sim 0.8 |e|$ to this specific CMO. In a zeroth-order picture, this CMO can be approximated as two nonbonding V $3d$ electrons, one for each V center.

Likewise, HOMO–2 has an 82% component from V $3d_{x^2-y^2}$ AOs, also being balanced by a minor B $2p_z$ component. As a zeroth-order approximation, the CMO may be classified as two nonbonding V $3d$ electrons as well, one for each V center. The AdNDP scheme (Figure 4d) gives ON values of $1.66 |e|$, which are partitioned as two-center nonbonding elements. These ONs are in line with the CMO component data. In short, subset (d) can be approximated as four nonbonding V $3d$ electrons (with secondary bonding effect as mediated by the B_7 ring). Each V center in the inverse sandwich cluster has two nonbonding $3d$ electrons, although they do not represent a lone pair.

It is important to comment that HOMO–1 and HOMO–2 in Figure 3d should not be confused with the π sextet in Figure 3b. They are fundamentally different types of CMOs. Specifically, HOMO–4/HOMO–3/HOMO–10 in subset (b) of Figure 3 are dominated by B $2p_z$ AOs, with contributions that amount to 88.4% , 88.2% , and 74.5% , respectively. In stark contrast, HOMO–1 and HOMO–2 in subset (d) are primarily V-based as described

above, with relatively minor contributions from B $2p_z$ AOs of 17.1% and 16.2%, respectively. These CMO component data differ distinctly. One should never consider 88.4%, 88.2%, 74.5%, 17.1%, and 16.2% as a single series of values. It would be conceptually incorrect to assign these five CMOs collectively as a 10π system, even though they seem to satisfy the $(4n + 2)$ Hückel electron counting for π aromaticity. Such a claim of 10π aromaticity should not appear in the literature, for the sake of science.

For another technical comment, the relatively low ON values of 1.66 $|e|$ in Figure 4d are natural, as long as one partitions them as 2c-2e nonbonding elements. The exact nature of their corresponding CMOs, that is, subset (d) in Figure 3, are fully described in the text. To consider these as 2c-2e nonbonding elements is only an approximation, as explicitly stated. In order to rationally evaluate how good such an approximation is, one may compare a two-center ON value of 1.66 $|e|$ with an ideal nine-center ON value of 2.00 $|e|$. Note that the ratio of contribution from a B center and a V center herein is about 1:17. It is mentioned that AdNDP is a user-directed tool for bonding analysis, and the interpretation of its output requires expertise. One should not solely rely on the AdNDP data in order to understand a molecular system.

Last but not least, subset (e) in Figure 3 has one CMO, that is, the HOMO, which largely originates from V $3d_z^2$ AOs from the V_2 dimer with a collective contribution of 55.3%. In this CMO, the V $3d_z^2$ AOs from two V sites are combined in a constructive, head-to-head manner with an apparent spatial overlap, owing to the short V–V distance (2.34 Å; see Section 2.2), which justifies direct V–V σ bonding in the inverse sandwich. The HOMO can be, therefore, roughly classified as a bonding CMO within the V_2 dimer. To further assess metal–metal bonding in the system, a constructive/destructive recombination can technically be pursued between a pair of CMOs: HOMO and HOMO–7. Note that HOMO–7 also has a nonnegligible yet slightly smaller component of V $3d_z^2$ AOs (by 42.4%). Thus, HOMO and HOMO–7 are indeed a pair of CMOs that are responsible for V–V bonding in the system. The constructive/destructive recombination of the pair is schematically illustrated in Figure S4.

The outcome is presented in Figure 6. Here, HOMO–7 is “purified”, upon destructive recombination with HOMO, as a completely bonding CMO, which is strictly seven-centered in nature along the B_7 ring (Figure 6b) and remains a component of the aromatic σ sextet. Likewise, upon constructive recombination with HOMO–7, HOMO is further strengthened for direct V–V σ bonding. This bonding element (Figure 6a) is purely two-centered in nature and solely situated on the V_2 dimer, which has a spatial shape that shows straightforward evidence for bonding overlap between the V $3d_z^2$ AOs from two V centers in a σ -bond manner. The ON value for this σ bond may be obtained from the AdNDP scheme, which is 1.99 $|e|$ (Figure 4e), a perfect number. In short, our analysis clearly establishes an ideal, direct V–V σ single bond in inverse sandwich GM C_s ($^1A'$) $V_2B_7^-$ cluster. This result is remarkable and rather conclusive.

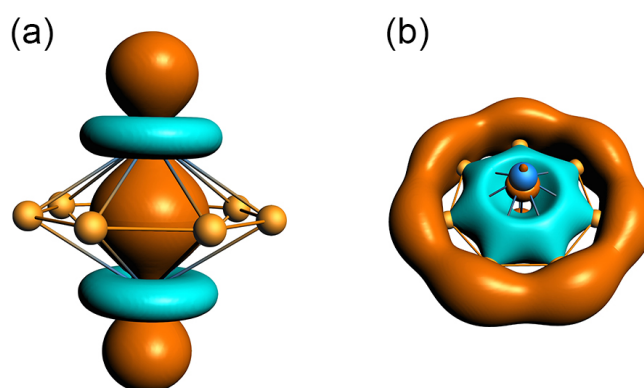


Figure 6. Two isolated and purified σ bonds associated with a pair of CMOs (HOMO and HOMO–7) in GM C_s $V_2B_7^-$ cluster. (a) One Lewis-type 2c-2e V–V d_σ single bond. (b) One delocalized σ bond along the B_7 ring. The latter is part of the aromatic σ sextet.

3.3. Electronic Transmutation: Analogy between an Inverse Sandwich Cluster and a Planar Molecular Wheel Cluster

The inverse sandwich GM C_s ($^1A'$) $V_2B_7^-$ cluster is quite unusual in terms of structure. It contains a monocyclic B_7 ring and a perpendicularly penetrating V_2 dimer. A monocyclic B_7 ring is not present in bare boron clusters. A real V_2 dimer with a Lewis-type V–V σ single bond is a rare example in inverse sandwich clusters. The seven-fold in-plane hypercoordination in the cluster suggests that the $6\pi/6\sigma$ frameworks are truly delocalized, thus rendering double π/σ aromaticity. To rationalize these peculiar aspects of the title inverse sandwich cluster, we would like to offer further discussion here. Our key idea is to introduce the concept of “electronic transmutation” [31,32] to the present system.

Specifically, the V_2 unit in the system is, chemically rather than only physically, a genuine dimer. The chemical identity of the V_2 dimer is established by a perfect Lewis-type σ single bond (Figure 6a). Thus, the V_2 dimer should be capable of participating in chemical bonding as a single chemical unit, such as an individual atom. In terms of the number of valence electrons for the V_2 dimer (Figure 4d,e), six electrons are consumed either as nonbonding electrons (two for each V site) or a Lewis σ single bond. The latter σ bond involves the contribution from an extra charge in the HOMO (Figures 3e and 6a). In the context of bonding in an inverse sandwich cluster, a Lewis V–V σ single bond is relatively localized, which is therefore sort of equivalent to a lone pair in an atomic site. With this understanding, the V_2 dimer, formally in its $[V_2]^-$ charge-state, is effectively valence five in terms of its capacity to participate in chemical bonding in the inverse sandwich system, because 6 out of its 11 electrons are actually “locked” or localized inside the dimer. In other words, the $[V_2]^-$ dimer in GM C_s ($^1A'$) $V_2B_7^-$ cluster is transformed to a single C^- or B^{2-} site via electronic transmutation. As a consequence, the GM $V_2B_7^-$ cluster becomes chemically analogous to a D_{7h} CB_7^- or B_8^{2-} cluster [3,5,6,40]. Note that the formal charge state and the NBO charges should not be confused with each other; the latter are due to the polar nature of V–B bonding in the alloy system (see Section 2.2). In this way, a boron-based inverse sandwich cluster can be chemically equivalent to a planar molecular wheel system, which is an exotic chemical connection in the field.

A comparison between the present GM $V_2B_7^-$ cluster and a model B_8^{2-} cluster is presented in Figure 7. The delocalized π/σ CMOs of the two systems show close one-to-one correspondence with each other, as do their skeleton σ bonds (not shown). Note that HOMO–10, HOMO–5, HOMO–6, and HOMO–7 have components of 18.8%, 30.3%, 30.5%, and 42.4% V 3d AOs from the V_2 dimer, respectively. Briefly, the five valence electrons from V_2 dimer participate in three-fold bonding in the inverse sandwich. They contribute to skeleton σ bonding by approximately $\sim 1.7 |e|$ and to delocalized 6σ framework by $\sim 2.1 |e|$, whereas their contribution to delocalized 6π framework is relatively minor ($\sim 0.4 |e|$). This bonding pattern is identical to that of a model D_{7h} CB_7^- cluster, in that the $[V_2]^-$ or C^- center is truly valence five (Figure 8b).

Nevertheless, GM C_s $V_2B_7^-$ and D_{7h} B_8^{2-} clusters show a subtle difference in the spatial distribution of their valence electrons. According to the natural atomic charges from NBO analysis [35], the two extra electrons in model B_8^{2-} cluster are exclusively located on the B_7 ring (Figure 8c), suggesting that it is best described as a neutral B center surrounded by a dianionic B_7^{2-} ring, in which the hypercoordinate B center is actually valence three (rather than as B^{2-}). Also shown in Figure 8 are the natural atomic charges in neutral C_s V_2B_7 cluster. A comparison between GM C_s $V_2B_7^-$ (Figure 2) and C_s V_2B_7 (Figure 8a) clusters indicates that the extra charge in the anion is largely located on two V centers. This statement appears to be appropriate for at least two reasons. Firstly, the NBO charge on a V center changes from $+1.01 |e|$ in the neutral to $+0.43 |e|$ in the anion. In other words, upon addition of an extra electron, the V_2 dimer gains over $\sim 1.1 |e|$ (including electronic relaxation or redistribution, of course). Second, the HOMO of GM C_s $V_2B_7^-$ cluster is mainly based on the V_2 dimer (see Figures 3e, 4e and 6a), in which the extra electron in anion cluster occupies. Furthermore, the V–V distance in C_s V_2B_7 cluster is expanded to 2.54 Å (relative to 2.34 Å in GM $V_2B_7^-$ cluster). This expansion is yet another

piece of evidence for direct V–V σ bonding in GM C_s $V_2B_7^-$ cluster. In neutral C_s V_2B_7 cluster, only five electrons are “locked” inside the V_2 unit, because its HOMO is now only half-occupied. This observation further shows that the V_2 unit is valence five in terms of bonding in the inverse sandwiches. It is reiterated that the net NBO charge of 1.01 |e| on a V center in C_s V_2B_7 cluster is due to the polar nature of V–B bonding. Therefore, an interesting implication from C_s V_2B_7 cluster is that the V–B bonding in inverse sandwich clusters do have a marked ionic component, despite bonding covalency.

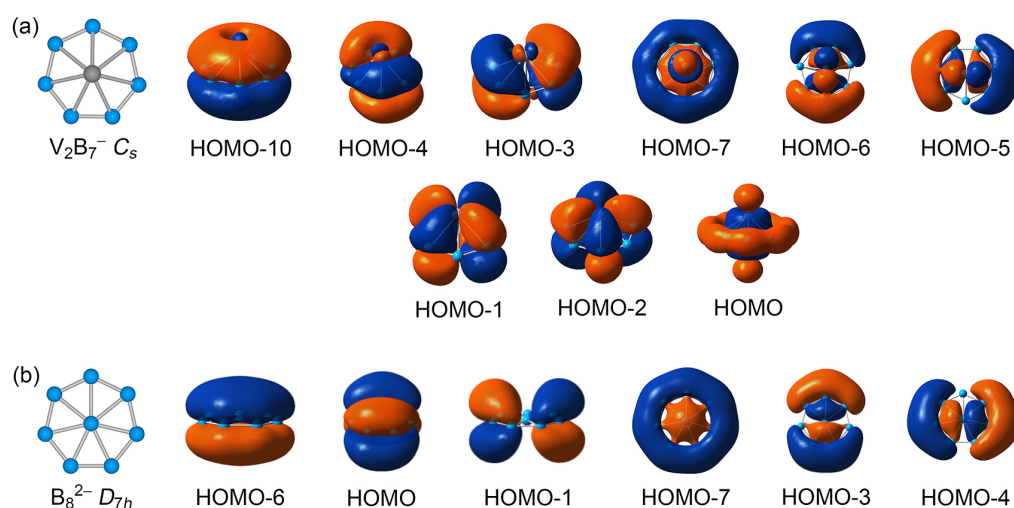


Figure 7. Comparison of delocalized π/σ CMOs of (a) GM C_s $V_2B_7^-$ cluster with those of (b) a model D_{7h} B_8^{2-} dianion cluster. The systems are not strictly isoelectronic to each other, because the former has six more valence electrons; see the three extra CMOs in (a). Nonetheless, these two systems are isovalent in terms of peripheral B–B σ bonds and delocalized $6\pi/6\sigma$ frameworks, which collectively consume a total of 26 electrons.

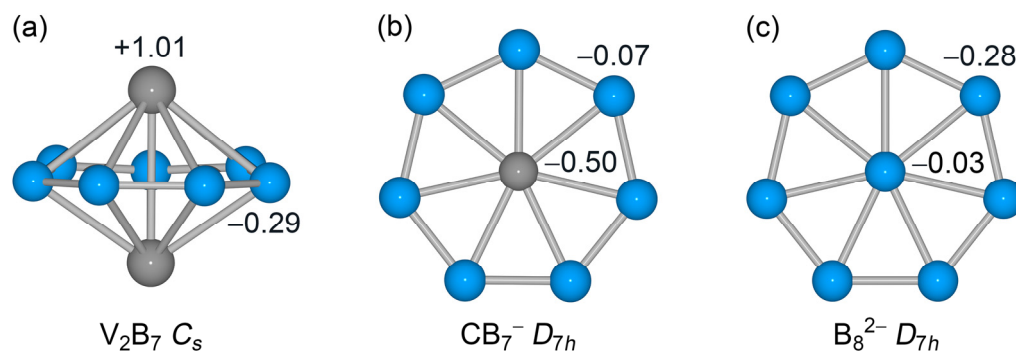


Figure 8. Calculated natural atomic charges (in |e|) for (a) neutral C_s V_2B_7 , (b) model D_{7h} CB_7^- , and (c) model D_{7h} B_8^{2-} clusters. The above data are obtained from natural bond orbital (NBO 6.0) analysis at the PBE0/def2-qzvp level.

It should be noted that the involvement of V_2 dimer in three-fold chemical bonding in the inverse sandwich is a crucial factor that helps stabilize the binary system, which is also a demonstration of V–B bonding covalency in the cluster. While the contribution of electrons from a specific site may differ in $V_2B_7^-$, CB_7^- , and B_8^{2-} clusters, the three systems share the same 14 skeleton electrons, 6π aromaticity, and 6σ aromaticity. The systems only differ by three extra CMOs in $V_2B_7^-$ cluster, as depicted in the second row in Figure 7a, which are primarily confined inside the V_2 unit as nonbonding electrons or a Lewis-type V–V σ bond, as analyzed above. It is the general bonding pattern that chemically connects these systems, which validates the concept of electronic transmutation in the inverse sandwich cluster. We note that the present case is a fairly new type of electronic transmutation.

4. Methods Section

The GM structure of $V_2B_7^-$ cluster was established in this work using the Coalescence Kick (CK) searches [41,42] at the PBE0/LANL2DZ level, which was also aided by manual structure constructions. The CK algorithm is believed to be capable of doing “mindless chemistry” [42], which is more than sufficiently powerful for the current simple alloy cluster system. A total of 3000 stationary points were probed on the singlet-state potential energy surface of the system, as were 3000 triplet-state geometries. The first 30 lowest-energy isomeric structures were then fully reoptimized at the PBE0/def2-qzvp level. Vibrational frequencies were also analyzed at the same level to ensure that the reported structures are true minima on the potential energy surface. The relative energies of all isomers presented in this paper were corrected for the ZPEs.

In order to check for computational consistency of the DFT methods in geometries and energetics, we made further efforts for the current cluster system. Firstly, the top 15 low-lying isomers were recalculated at the PBE0-D3/def2-qzvp level, which served to examine the dispersion effect. Such an effect turned out to be insignificant for the present system. Second, different density functionals were checked using independent and comparative computational data at the B3LYP/def2-qzvp level, also for the first 15 alternative structures. It is stressed that the PBE0 and B3LYP approaches are generally considered to be complementary to each other in quantum chemistry. The above extra efforts also included vibrational frequency analyses as well as ZPE corrections for energetics. Thus, the three levels of theory should collectively lead to rather solid conclusions for the present system. All three levels of theory reached the same GM structure for $V_2B_7^-$ cluster. Since the three sets of computational data are highly coherent, we primarily focus on the PBE0 data in this paper.

The WBIs and natural atomic charges were calculated using the NBO analysis (NBO 6.0) [35,43], which was completed at the PBE0/def2-qzvp level. Chemical bonding was elucidated using CMO analysis, as well as AdNDP [36] and ELF analyses [38,39]. To independently evaluate aromaticity, NICSs [37] were calculated at PBE0/def2-qzvp. The CMO compositions were analyzed using the Multiwfn program [44]. The AdNDP data were visualized using Molekel [45]. All the electronic structure calculations were accomplished using the Gaussian 09 program [46].

5. Conclusions

We have computationally designed a new example of boron-based inverse sandwich clusters, C_s ($^1A'$) $V_2B_7^-$, through unbiased global-minimum (GM) structure searches and quantum chemical calculations. It is close to a highly symmetric D_{7h} system. The GM cluster features a monocyclic B_7 ring on the periphery and a perpendicularly penetrating V_2 dimer. The V sites have seven-fold hypercoordination with boron in a quasi-planar fashion. The inverse sandwich cluster is governed by double $6\pi/6\sigma$ aromaticity, following the $(4n + 2)$ Hückel rule. The skeleton σ bonding in the system involves a marked contribution from the V_2 dimer, which should be best described as a set of roof-like, four-center two-electron ($4c-2e$) $V-B_2-V$ σ bonds, rather than strict Lewis-type $2c-2e$ B–B σ single bonds. Interesting, the V_2 dimer possesses a genuine $2c-2e$ V–V σ bond and represents a rare case of direct metal–metal bonding in inverse sandwich clusters. Despite its 11 valence electrons, the V_2 dimer in its formal $[V_2]^-$ charge state in the alloy cluster is chemically analogous to a single atom with valence five, such as a C^- or B^{2-} site. This is a new type of “electronic transmutation”. The remaining six electrons in the V_2 dimer are merely present as spectators in terms of chemical bonding within the inverse sandwich, including four nonbonding electrons and a Lewis-type V–V σ bond. Note that in the corresponding neutral inverse sandwich C_s V_2B_7 cluster, the V_2 unit is also effectively valence five in terms of global chemical bonding. The anionic and neutral clusters only differ in their V–V σ bonding; that is, a σ single bond versus a σ half bond. The above understanding offers a natural connection between an inverse sandwich cluster and a planar hypercoordinate molecular wheel, such as that between $V_2B_7^-$, CB_7^- , and B_8^{2-} clusters. It is believed

that the concept of electronic transmutation may be further developed to elucidate novel molecular structures and gain new physical chemistry.

Supplementary Materials: The following supporting information can be downloaded at: <https://www.mdpi.com/article/10.3390/molecules28124721/s1>, Table S1: Cartesian coordinates for GM C_s ($^1A'$) and D_{7h} ($^1A_1'$) structures of $V_2B_7^-$ cluster at the PBE0/def2-qzvp level; Table S2: Calculated bond distances and Wiberg bond indices (WBIs) of GM C_s ($^1A'$) and D_{7h} ($^1A_1'$) structures at PBE0/def2-qzvp; Figure S1: Alternative optimized low-lying isomeric structures of $V_2B_7^-$ cluster at PBE0/def2-qzvp, along with their relative energies at three levels of theory; Figure S2: An alternative bonding scheme of GM $V_2B_7^-$ cluster based on AdNDP analysis; Figure S3: NICS_{zz} data for GM $V_2B_7^-$ cluster at PBE0/6-311+G*; Figure S4: Schematic presentation of constructive/destructive recombination between HOMO and HOMO-7 of GM $V_2B_7^-$ cluster that generates a “purified” Lewis-type V-V σ single bond.

Author Contributions: Conceptualization, H.-J.Z.; methodology, P.-F.H., Q.S. and H.-J.Z.; software, P.-F.H.; validation, P.-F.H. and H.-J.Z.; investigation, P.-F.H.; writing—original draft preparation, P.-F.H.; writing—review and editing, H.-J.Z.; supervision, H.-J.Z. and Q.S.; funding acquisition, H.-J.Z. All authors have read and agreed to the published version of the manuscript.

Funding: This work was supported by the National Natural Science Foundation of China under grant nos. 21873058, 21573138, and 22173053.

Institutional Review Board Statement: Not applicable.

Informed Consent Statement: Not applicable.

Data Availability Statement: The data from this work are available in the manuscript as well as in the electronic Supplementary Materials file.

Conflicts of Interest: The authors declare no conflict of interest.

References

1. Lipscomb, W.N. The boranes and their relatives. *Science* **1977**, *196*, 1047–1055. [[CrossRef](#)]
2. Hanley, L.; Whitten, J.L.; Anderson, S.L. Collision-induced dissociation and ab initio studies of boron cluster ions: Determination of structures and stabilities. *J. Phys. Chem.* **1988**, *92*, 5803–5812. [[CrossRef](#)]
3. Zhai, H.-J.; Alexandrova, A.N.; Birch, K.A.; Boldyrev, A.I.; Wang, L.-S. Hepta- and octacoordinate boron in molecular wheels of eight- and nine-atom boron clusters: Observation and confirmation. *Angew. Chem. Int. Ed.* **2003**, *42*, 6004–6008. [[CrossRef](#)] [[PubMed](#)]
4. Zhai, H.-J.; Kiran, B.; Li, J.; Wang, L.-S. Hydrocarbon analogues of boron clusters—Planarity, aromaticity and antiaromaticity. *Nat. Mater.* **2003**, *2*, 827–833. [[CrossRef](#)]
5. Alexandrova, A.N.; Boldyrev, A.I.; Zhai, H.-J.; Wang, L.-S. All-boron aromatic clusters as potential new inorganic ligands and building blocks in chemistry. *Coord. Chem. Rev.* **2006**, *250*, 2811–2866. [[CrossRef](#)]
6. Zubarev, D.Y.; Boldyrev, A.I. Comprehensive analysis of chemical bonding in boron clusters. *J. Comput. Chem.* **2007**, *28*, 251–268. [[CrossRef](#)] [[PubMed](#)]
7. Sergeeva, A.P.; Zubarev, D.Y.; Zhai, H.-J.; Boldyrev, A.I.; Wang, L.-S. A photoelectron spectroscopic and theoretical study of B_{16}^- and B_{16}^{2-} : An all-boron naphthalene. *J. Am. Chem. Soc.* **2008**, *130*, 7244–7246. [[CrossRef](#)]
8. Huang, W.; Sergeeva, A.P.; Zhai, H.-J.; Averkiev, B.B.; Wang, L.-S.; Boldyrev, A.I. A concentric planar doubly π -aromatic B_{19}^- cluster. *Nat. Chem.* **2010**, *2*, 202–206. [[CrossRef](#)]
9. Sergeeva, A.P.; Piazza, Z.A.; Romanescu, C.; Li, W.-L.; Boldyrev, A.I.; Wang, L.-S. B_{22}^- and B_{23}^- : All-boron analogues of anthracene and phenanthrene. *J. Am. Chem. Soc.* **2012**, *134*, 18065–18073. [[CrossRef](#)]
10. Li, W.-L.; Zhao, Y.-F.; Hu, H.-S.; Li, J.; Wang, L.-S. $[B_{30}]^-$: A quasiplanar chiral boron cluster. *Angew. Chem. Int. Ed.* **2014**, *53*, 5540–5545. [[CrossRef](#)]
11. Piazza, Z.A.; Hu, H.-S.; Li, W.-L.; Zhao, Y.-F.; Li, J.; Wang, L.-S. Planar hexagonal B_{36} as a potential basis for extended single-atom layer boron sheets. *Nat. Commun.* **2014**, *5*, 3113. [[CrossRef](#)]
12. Zhai, H.-J.; Zhao, Y.-F.; Li, W.-L.; Chen, Q.; Bai, H.; Hu, H.-S.; Piazza, Z.A.; Tian, W.-J.; Lu, H.-G.; Wu, Y.-B.; et al. Observation of an all-boron fullerene. *Nat. Chem.* **2014**, *6*, 727–731. [[CrossRef](#)] [[PubMed](#)]
13. Li, W.-L.; Chen, Q.; Tian, W.-J.; Bai, H.; Zhao, Y.-F.; Hu, H.-S.; Li, J.; Zhai, H.-J.; Li, S.-D.; Wang, L.-S. The B_{35} cluster with a double-hexagonal vacancy: A new and more flexible structural motif for borophene. *J. Am. Chem. Soc.* **2014**, *136*, 12257–12260. [[CrossRef](#)] [[PubMed](#)]
14. Wang, Y.-J.; Zhao, Y.-F.; Li, W.-L.; Jian, T.; Chen, Q.; You, X.-R.; Ou, T.; Zhao, X.-Y.; Zhai, H.-J.; Li, S.-D.; et al. Observation and characterization of the smallest borospherene: B_{28}^- and B_{28} . *J. Chem. Phys.* **2016**, *144*, 064307. [[CrossRef](#)] [[PubMed](#)]

15. Oger, E.; Crawford, N.R.M.; Kelting, R.; Weis, P.; Kappes, M.M.; Ahlrichs, R. Boron cluster cations: Transition from planar to cylindrical structures. *Angew. Chem. Int. Ed.* **2007**, *46*, 8503–8506. [[CrossRef](#)]
16. Kiran, B.; Bulusu, S.; Zhai, H.-J.; Yoo, S.; Zeng, X.-C.; Wang, L.-S. Planar-to-tubular structural transition in boron clusters: B₂₀ as the embryo of single-walled boron nanotubes. *Proc. Natl. Acad. Sci. USA* **2005**, *102*, 961–964. [[CrossRef](#)]
17. Romanescu, C.; Galeev, T.R.; Li, W.-L.; Boldyrev, A.I.; Wang, L.-S. Aromatic metal-centered monocyclic boron rings: CoB₈[−] and RuB₉[−]. *Angew. Chem. Int. Ed.* **2011**, *50*, 9334–9337. [[CrossRef](#)]
18. Popov, I.A.; Li, W.-L.; Piazza, Z.A.; Boldyrev, A.I.; Wang, L.-S. Complexes between planar boron clusters and transition metals: A photoelectron spectroscopy and ab initio study of CoB₁₂[−] and RhB₁₂[−]. *J. Phys. Chem. A* **2014**, *118*, 8098–8105. [[CrossRef](#)]
19. Popov, I.A.; Jian, T.; Lopez, G.V.; Boldyrev, A.I.; Wang, L.-S. Cobalt-centered boron molecular drums with the highest coordination number in the CoB₁₆[−] cluster. *Nat. Commun.* **2015**, *6*, 8654. [[CrossRef](#)]
20. Li, W.-L.; Chen, X.; Jian, T.; Chen, T.-T.; Li, J.; Wang, L.-S. From planar boron clusters to borophenes and metalloborophenes. *Nat. Rev. Chem.* **2017**, *1*, 0071. [[CrossRef](#)]
21. Jian, T.; Chen, X.; Li, S.-D.; Boldyrev, A.I.; Li, J.; Wang, L.-S. Probing the structures and bonding of size-selected boron and doped-boron clusters. *Chem. Soc. Rev.* **2019**, *48*, 3550–3591. [[CrossRef](#)]
22. Romanescu, C.; Galeev, T.R.; Li, W.-L.; Boldyrev, A.I.; Wang, L.-S. Understanding boron through size-selected clusters: Structure, chemical bonding, and fluxionality. *Acc. Chem. Res.* **2014**, *47*, 1349–1358.
23. Li, W.-L.; Romanescu, C.; Galeev, T.R.; Piazza, Z.A.; Boldyrev, A.I.; Wang, L.-S. Transition-metal-centered nine-membered boron rings: M@B₉ and M@B₉[−] (M = Rh, Ir). *J. Am. Chem. Soc.* **2012**, *134*, 165–168. [[CrossRef](#)]
24. Galeev, T.R.; Romanescu, C.; Li, W.-L.; Wang, L.-S.; Boldyrev, A.I. Observation of the highest coordination number in planar species: Decacoordinated Ta@B₁₀[−] and Nb@B₁₀[−] anions. *Angew. Chem. Int. Ed.* **2012**, *51*, 2101–2105. [[CrossRef](#)] [[PubMed](#)]
25. Zhai, H.-J.; Wang, L.-S.; Zubarev, D.Y.; Boldyrev, A.I. Gold apes hydrogen. The structure and bonding in the planar B₇Au₂[−] and B₇Au₂ clusters. *J. Phys. Chem. A* **2006**, *110*, 1689–1693. [[CrossRef](#)]
26. Xie, L.; Li, W.-L.; Romanescu, C.; Huang, X.; Wang, L.-S. A photoelectron spectroscopy and density functional study of di-tantalum boride clusters: Ta₂B_x[−] (x = 2–5). *J. Chem. Phys.* **2013**, *138*, 034308. [[CrossRef](#)] [[PubMed](#)]
27. Jia, J.-F.; Li, X.-R.; Li, Y.-A.; Ma, L.-J.; Wu, H.-S. Density functional theory investigation on the structure and stability of Sc₂B_n (n = 1–10) clusters. *Comput. Theo. Chem.* **2014**, *1027*, 128–134. [[CrossRef](#)]
28. Li, W.-L.; Xie, L.; Jian, T.; Romanescu, C.; Huang, X.; Wang, L.-S. Hexagonal bipyramidal [Ta₂B₆]^{−/0} clusters: B₆ rings as structural motifs. *Angew. Chem. Int. Ed.* **2014**, *53*, 1288–1292. [[CrossRef](#)]
29. Li, W.-L.; Chen, T.-T.; Xing, D.-H.; Chen, X.; Li, J.; Wang, L.-S. Observation of highly stable and symmetric lanthanide octa-boron inverse sandwich complexes. *Proc. Natl. Acad. Sci. USA* **2018**, *115*, E6972–E6977. [[CrossRef](#)]
30. Zhang, Y.; Zhao, X.Y.; Yan, M.; Li, S.-D. From inverse sandwich Ta₂B₇⁺ and Ta₂B₈ to spherical trihedral Ta₃B₁₂[−]: Prediction of the smallest metallo-borospherene. *RSC Adv.* **2020**, *10*, 29320–29325. [[CrossRef](#)]
31. Olson, J.K.; Boldyrev, A.I. Electronic transmutation: Boron acquiring an extra electron becomes ‘carbon’. *Chem. Phys. Lett.* **2012**, *523*, 83–86. [[CrossRef](#)]
32. Zhang, X.; Lundell, K.A.; Olson, J.K.; Bowen, K.H.; Boldyrev, A.I. Electronic transmutation (ET): Chemically turning one element into another. *Chem. Eur. J.* **2018**, *24*, 9200–9210. [[CrossRef](#)] [[PubMed](#)]
33. Pyykkö, P. Additive covalent radii for single-, double-, and triple-bonded molecules and tetrahedrally bonded crystals: A summary. *J. Phys. Chem. A* **2015**, *119*, 2326–2337. [[CrossRef](#)] [[PubMed](#)]
34. Li, S.-D.; Zhai, H.-J.; Wang, L.-S. B₂(BO)₂^{2−}—Diboronyl diborene: A linear molecule with a triple boron-boron bond. *J. Am. Chem. Soc.* **2008**, *130*, 2573–2579. [[CrossRef](#)] [[PubMed](#)]
35. Reed, A.E.; Curtiss, L.A.; Weinhold, F. Intermolecular interactions from a natural bond orbital, donor-acceptor viewpoint. *Chem. Rev.* **1988**, *88*, 899–926. [[CrossRef](#)]
36. Zubarev, D.Y.; Boldyrev, A.I. Developing paradigms of chemical bonding: Adaptive natural density partitioning. *Phys. Chem. Chem. Phys.* **2008**, *10*, 5207–5217. [[CrossRef](#)]
37. Chen, Z.; Wannere, C.S.; Corminboeuf, C.; Puchta, R.; Schleyer, P.v.R. Nucleus-independent chemical shifts (NICS) as an aromaticity criterion. *Chem. Rev.* **2005**, *105*, 3842–3888. [[CrossRef](#)]
38. Poater, J.; Duran, M.; Solà, M.; Silvi, B. Theoretical evaluation of electron delocalization in aromatic molecules by means of atoms in molecules (AIM) and electron localization function (ELF) topological approaches. *Chem. Rev.* **2005**, *105*, 3911–3947. [[CrossRef](#)]
39. Silvi, B.; Savin, A. Classification of chemical bonds based on topological analysis of electron localization functions. *Nature* **1994**, *371*, 683–686. [[CrossRef](#)]
40. Wang, L.-M.; Huang, W.; Averkiev, B.B.; Boldyrev, A.I.; Wang, L.-S. CB₇[−]: Experimental and theoretical evidence against hypercoordinate planar carbon. *Angew. Chem. Int. Ed.* **2007**, *46*, 4550–4553. [[CrossRef](#)]
41. Saunders, M. Stochastic search for isomers on a quantum mechanical surface. *J. Comput. Chem.* **2004**, *25*, 621–626. [[CrossRef](#)] [[PubMed](#)]
42. Bera, P.P.; Sattelmeyer, K.W.; Saunders, M.; Schaefer, H.F., III; Schleyer, P.v.R. Mindless chemistry. *J. Phys. Chem. A* **2006**, *110*, 4287–4290. [[CrossRef](#)] [[PubMed](#)]
43. Glendening, E.D.; Badenhoop, J.K.; Reed, A.E.; Carpenter, J.E.; Bohmann, J.A.; Morales, C.M.; Landis, C.R.; Weinhold, F. *NBO 6.0*; Theoretical Chemistry Institute, University of Wisconsin: Madison, WI, USA, 2013.
44. Lu, T.; Chen, F.-W. Multiwfn: A multifunctional wavefunction analyzer. *J. Comput. Chem.* **2012**, *33*, 580–592. [[CrossRef](#)] [[PubMed](#)]

45. Varetto, U. *Molekel 5.4.0.8*; Swiss National Supercomputing Center: Manno, Switzerland, 2009.
46. Frisch, M.J.; Trucks, G.W.; Schlegel, H.B.; Scuseria, G.E.; Robb, M.A.; Cheeseman, J.R.; Scalmani, G.; Barone, V.; Mennucci, B.; Petersson, G.A.; et al. *GAUSSIAN 09, Revision D.01*; Gaussian, Inc.: Wallingford, CT, USA, 2009.

Disclaimer/Publisher's Note: The statements, opinions and data contained in all publications are solely those of the individual author(s) and contributor(s) and not of MDPI and/or the editor(s). MDPI and/or the editor(s) disclaim responsibility for any injury to people or property resulting from any ideas, methods, instructions or products referred to in the content.